Acta Montanistica Slovaca
ISSN 1335-1788
actamont.tuke.sk

Advances in Shear-Seepage Properties of Rock Mass Filled with Joint Fissure

Jiyun ZHANG[1], Shuren WANG[2], Yunxing CAO[3], Weibin MA[4], Zhichao LI[5]* and *Wenxue CHEN[6]*

Authors' affiliations and addresses:
[1] School of Civil Engineering, Henan Polytechnic University, Jiaozuo 454003, China
e-mail: 465743184@qq.com

[2] School of Civil Engineering, Henan Polytechnic University, Jiaozuo 454003, China
e-mail: shurenwang@hpu.edu.cn

[3] Institute of Resources and Environment, Henan Polytechnic University, Jiaozuo 454003, China
e-mail: yxcao17@126.com

[4] Railway Engineering Research Institute, China Academy of Railway Sciences Corporation Limited, Beijing 100081, China
e-mail: dwangfei@163.com

[5] School of Civil Engineering, Henan Polytechnic University, Jiaozuo 454003, China
e-mail: zhichaoli@hpu.edu.cn

[6] Department of Civil & Building Engineering, University of Sherbrooke, Sherbrooke J1K 2R1, Canada
e-mail: Wenxue.chen@usherbrooke.ca

***Correspondence:**
Shuren Wang, International Joint Research Laboratory of Henan Province for Underground Space Development and Disaster Prevention, Jiaozuo 454003, China
tel.:+86 15738529570
e-mail: shurenwang@hpu.edu.cn

Funding information:
Key Project of Natural Science Foundation of Henan Province (232300421134), and Zhongyuan Science and Technology Innovation Leading Talent Program (244200510005), China.

Acknowledgement:
The authors would like to express their sincere gratitude to the editor and reviewers for their valuable comments, which have greatly improved this paper.

How to cite this article:
Zhang, J.Y., Wang, S.R., Cao, Y.X., Ma, W.B., Li, Z.C., and Chen, W.X. (2023). Advances in shear-seepage properties of rock mass filled with joint fissure. *Acta Montanistica Slovaca*, Volume 28 (4), 834-849

DOI:
https://doi.org/10.46544/AMS.v28i4.04

Abstract
Since joint fissures are distributed extensively within rock masses, rock masses evolve into "sandwich" shapes when filled with joint fissures under long-term geological action, which causes rock discontinuities and destroys rock stability. This study reviews the advances in the shear-seepage properties of rock masses filled with joint fissures (RMFJFs) under static, quasistatic, and dynamic loads, including laboratory experiments, theoretical analysis, and numerical calculations. Results show that the shear properties of RMFJFs are closely associated with the strength of the fillings, the filling degree, and the roughness of the joints. RMFJFs develop under the stress of surrounding rocks, and their seepage properties are therefore affected by the surrounding stress and the filling degree, the rock layer thickness, and the porosity of the rock or fillings. However, detailed studies on the seepage properties of RMFJFs under cyclic loading, impact loading, and different shear rates are lacking. Finally, the existing problems in the research on the seepage properties of RMFJFs are clarified, a constructive research strategy is proposed, and the related trends are discussed in light of the overall mechanical behavior of RMFJFs.

Keywords
Rock mass, Joint fissures, Fillings, Shear-seepage characteristics, Cyclic loading.

Introduction

The 21st century is the right era to develop and utilize underground space. Geostress variation due to excavation can activate jointed fissures that exist extensively in underground rock masses and can exert various effects on underground engineering. Therefore, the effects of these jointed fissures are crucial to underground activities and deserve detailed study. The related research has become a hot topic.

Joint fissures are characterized by the randomness of the fissure aperture, attitudinal complexity, and uncertainty in strength, and thus, they have negative impacts on the evaluation of rock integrity and strength. In reality, jointed fissures can cause a series of disasters, such as dam failure, landslides, slope instability, and roadway roof instability, especially when they integrate with water flow. Moreover, jointed fissures can serve as channels for transporting oil, gas, and slurry. Therefore, they can improve the extraction efficiency of hydrocarbon resources, increase the rock strength in tunnel supports, and represent an active characteristic.

Joint fissures can open and close circularly under tectonic stress. These fissures can be classified into two categories: filled fissures and unfilled fissures. Fillings can affect a rock mass's mechanical character and reliability to some degree and can even lead to disasters. For example, the famous accident of the Malpasset Dam in France in 1959 drew extensive public concern for many years (Kyaw et al., 2023), in which jointed fissures contributed greatly to dam instability. This approach has changed the traditional way in which scholars use the continuum elastic-plastic theory to analyze rock mass stability and has helped to accelerate the study of the shear-seepage property of rock masses filled with joint fissures (RMFJFs).

This study mainly discusses the research status, clarifies the existing problems, and discusses the trend of the shear-seepage properties of RMFJFs through laboratory experiments, theoretical analysis, and numerical simulation.

Mechanical properties of RMFJF

Joint fractures can accelerate the evolution of rock mass failure, and the permeability of the damaged area improves the quantity of rock mass failure. The RMFJF consists of a parent rock mass and fillings, and the mechanical properties are divided into three cases according to the level of parent rock strength: greater than, equal to, and less than the fillings.

Theoretical model of RMFJF

Most studies on the shear strength of RMFJFs have been conducted by artificially creating regular dentate joints, injecting the fillings, and then conducting direct shear tests. The concept of the filling degree was introduced to the study of the RMFJF in 2006. Some academics have argued that when the filling degree is less than 100%, the intensity of the rock sample is fixed by the physical properties of both materials. When the filling degree was greater than 200%, the intensity was only determined by the feature of the fillings, for which the concept of the critical value of the filling degree needed to be considered. Papaliangas et al. (1993) reported that an increase in the filling degree causes a decrease in the shear strength of rock samples, and the critical value of the filling degree is largely determined by the physical behavior of the fillings. Premadasa and Indraratna (2020) discovered that the shear strength of an RMFJF filled with bentonite decreased substantially, and the magnitude of the filling degree affected the location of the shear slip; moreover, the filling degree and the physical properties of the fillings directly affected the sample failure modes, and the shear strength decreased as the thickness of the filling layer increased. Ladanyi (2006) considered the effect of the filling degree and classified shear damage into two forms. The corresponding equation of shear strength was as follows:

$$\tau_p = \begin{cases} \sigma_n \tan(i+\varphi_b) + \dfrac{c_u}{1-m\tan i_0 \tan\varphi_b} \\ m(R-C)+C \end{cases} \tag{1}$$

where σ_n is the positive stress; i_0 denotes the initial fluctuation angle; c_u represents the undrained shear intensity; and φ_b denotes the friction angle; m represents the reduction coefficient; i and R are the peak dilatancy angle, and the shear intensity of unfilled fractures, respectively; and C is the shear strength of the filling.

Premadasa and Indraratna (2020) reported that the ratio of the filling percentage to the critical value strongly influenced the damage pattern of samples when soft materials filled joint fissures, as shown in Fig. 1. Whether these results can be extended to natural jointed rock masses filled with hard material needs further study. Based on the results of Papaliangas et al. (1993), the shear intensity normalization model of the RMFJF was proposed, and the normalized shear strength was expressed as τ_p/t_n, which was equal to the algebraic sum of two functions, A and B. When the critical value of the filling degree $(t/\Delta)_{cr}$ maintained a certain value, the friction angle and undulation angle of the fracture surface had no effect on the shear intensity of the RMFJF as the value of function A decreased to zero. However, the level of function B increases continuously with increasing t/Δ to $(t/\Delta)_{cr}$. The

shear strength of the sample under these conditions was equal to that of the fillings when a constant value of this ratio was reached. Indraratna et al. have performed much work in this field, but we will not list their performance in detail. Here, t/Δ is the filling degree of the rock mass.

The Bandis empirical formula can characterize the variation in the shear intensity of the fracture surface, and it was modified by Qi et al. (2014) to obtain a theoretical formula for the shear and normal stiffness of the fracture surface. They found that the stiffness parameter of the joint surface was a function of stress, which is shown as follows:

$$\begin{cases} K_{st} = K_j(\sigma_n)^{n_j}\left(1 - f\left(\tau/\tau_p\right)\cdot R_f\right)^2, \tau \le \tau_p \\ f\left(\tau/\tau_p\right) = A\left(\tau/\tau_p\right)^2 + B\left(\tau/\tau_p\right) + C \\ \tau \le \tau_p \end{cases} \tag{2}$$

where K_{st} denotes the shear rigidity; n_j represents the shear rigidity index; R_f denotes the damage index; A, B, and C are constants; and τ and τ_p are the shear intensity and the peak shear intensity, respectively.

Filling fractures with soft materials can negatively affect the shear strength of the samples. Lu et al. (2017) created rock-like samples with cement as the joint filling material. The superposition effect of the parent rock on both sides of the joint was defined as S_1, the cementation effect of the rock-cement interface was defined as S_2 and the bearing effect of the cement nodular body was defined as S_3, as shown in Fig. 2. When the filling efficiency was less than 0.1, the shear strength and rigidity of the RMFJF increased linearly with increasing filling efficiency. When the filling efficiency was greater than 1.0, these mechanical parameters remained basically unchanged.

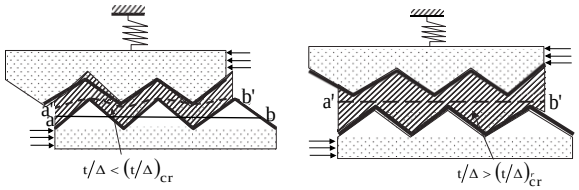

Fig. 1. Shear model of RMFJF (Ladanyi, 2006).

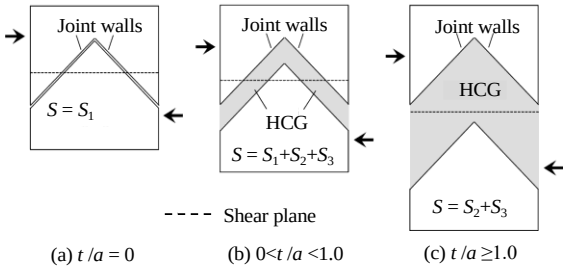

Fig. 2. Interaction between filling body and parent rock (Lu et al., 2017).

She and Sun (2018) presented a way to characterize the three-dimensional morphology of a fracture surface by three new variables independent of the measurement scale, I_{SRA} the fractal intercept, D_{SRA} the fractal dimension, and the mean coefficient of variation $\bar{C}_{VSR}$; subsequently, an empirical formula was created for the peak shear intensity of an RMFJF, as follows:

$$\begin{cases} \tau_p = \sigma_n \tan\left(i + \phi_b\right) + C_e \\ C_e = \dfrac{c\left(A_1/A_0\right)}{\cos i - \sin i \tan\phi_b} f(\lambda) \\ f(\lambda) = \left[\lambda/(\lambda + 0.1)\right]^n \end{cases} \tag{3}$$

where C_e denotes the effective cohesion; A_0 represents the area of the fracture surface; A_1 denotes the compression area of the fracture surface; λ denotes the filling degree of the joint; and $f(\lambda)$ is a function of the bonding degree.

Tian et al. (2018) obtained an empirical formula for the shear intensity of an RMFJF. Compared with the experimental results, the maximum deviation estimated through this formula was 0.185 MPa, and the minimum deviation was only 0.005 MPa.

Other studies proposed that the peak intensity of unfilled fractures (Yang et al., 2016a) can be written as:

$$\tau_p = \sigma_n \cdot \tan\left(\varphi_b + \frac{\theta^*_{\max}}{C^{0.45}} \cdot e^{-\frac{\sigma_n}{JCS}\cdot C^{0.75}}\right) \tag{4}$$

The peak intensity of a rock mass with a weakly filled joint can be expressed as:

$$\begin{cases} \tau_p = \sigma_n \cdot \tan\left(\varphi_b^{'} + \left(\dfrac{2}{1+\eta} \right)^{k_1} \cdot \dfrac{\theta_{\max}^{*}}{C^{0.45}} \cdot e^{-\frac{\sigma_n}{JCS^{'}} \cdot C^{0.75}} \right) \\ JCS^{'} = \sigma_g + (\sigma_r - \sigma_g) \cdot \left(\dfrac{\sigma_g}{\sigma_r + \sigma_g} \right)^{k_2} \end{cases} \tag{5}$$

The peak strength of samples with strongly filled fractures can be expressed as follows:

$$\begin{cases} \tau_p = C_0 \cdot e^{0.06\left(\frac{\theta_{max}^{*}}{C+1}\right)} + \sigma_n \cdot \tan\left(\varphi_b^{'} + (2/1+\eta)^{0.3} \cdot \dfrac{\theta_{max}^{*}}{C^{0.45}} \cdot e^{-\frac{\sigma_n}{JCS^{'}} \cdot C^{0.75}} \right) \\ JCS^{'} = \sigma_g + (\sigma_r - \sigma_g) \cdot \left(\dfrac{\sigma_g}{\sigma_r + \sigma_g} \right)^{1.45} \end{cases} \tag{6}$$

where *JCS'* represents the equivalent compressive strength; k_1 and k_2 represent the fitting parameters; and σ_g and σ_r are the compressive intensities of the filling and rock, respectively.

Chen et al. (2016) performed experiments on samples of joint rock with dilatant fillings. The authors divided the loading process according to the stress-strain curve into three stages: rheology, compaction, and elasticity. A mechanical model of an inverted Saint-Venant for an RMFJF with dilatant fillings was proposed, and the pre-peak constitutive equation of the sample was obtained.

$$\sigma = \begin{cases} \sigma_s, & (\varepsilon \le \varepsilon_s) \\ \sigma_s + \dfrac{\varepsilon - \varepsilon_s}{a + b(\varepsilon - \varepsilon_s)}, & (\varepsilon_s < \varepsilon < \varepsilon_b) \\ \sigma_s + E(\varepsilon - \varepsilon_s), & (\varepsilon > \varepsilon_b) \end{cases} \tag{7}$$

where σ_s is the yield limit; ε_s represents the plastic strain limit; and E denotes the equivalent modulus.

The effect of the fracture surface's contact situation on the sample's mechanical behavior was further investigated, and an incremental stress-displacement constitutive model of the RMFJF was constructed based on elastic-plasticity theory.

$$F = \tau_{pf} - \sigma_n \left[\tan(i + \varphi_b)(1-\kappa)^{\alpha} + \tan\varphi_{fill} \left(\frac{2}{1+1/\kappa} \right)^{\beta} \right] \tag{8}$$

where φ_{fill} denotes the rubbing angle of the filling material; and α and β represent material parameters, respectively.

The peak shear intensity criterion of the RMFJF is shown in Table 1.

Tab. 1. Peak shear intensity criterion of the RMFJF.

Name	Formula
Patton (Patton, 1996)	$\tau = \sigma_n \tan(\varphi_b + i)$
Barton (Barton, 1973)	$\tau = \sigma_n \tan\left[JRC \log_{10}(\sigma_c / \sigma_n) + \varphi_b \right]$
Min and Jing (Min and Jing, 2003)	$\tau = \sigma_n \tan\left(\varphi_b + i_0 (1 - \sigma_n / JCS)^k \right)$
Grasselli and Egger (Grasselli and Egger, 2003)	$\tau_p = \sigma_n \tan\varphi_r^{*}(1+g),\ \ g = \exp\left(-\dfrac{\theta_{\max}^{*}}{BA_0C} \dfrac{\sigma_n}{\sigma_t} \right)$
Son et al. (Son et al. 2004)	$\tau = \sigma_n \tan\left(\varphi_b + 1.44 i_{ave} (JCS/\sigma_n)^{0.116} \right)$
Xia et al. (Xia et al., 2003)	$\tau = \sigma_n \tan\left[\varphi_b + \dfrac{2R_s}{A_0} \dfrac{\overline{\theta_{3s}}}{1 + \sigma_n / 2A_0} \right]$

She and Sun (She and Sun, 2018)	$\tau_p = \sigma_n \tan(i + \varphi_b) + \frac{cA_{jq}}{A_{jj}(\cos i - \sin i \tan \varphi_b)}$
Zhang et al. (Zhang et al., 2015)	$\begin{cases} \tau = c_j(R_{JRC}, \sigma_n) + \sigma_n \tan[\varphi_j(R_{JRC}, \sigma_n)] \\ \varphi_j = 1.85 R_{JRC} \lg(25/\sigma_n) + 37.0 \end{cases}$
Zhang et al. (Zhang et al., 2012)	$\tau_p = \frac{\sigma_n \tan \varphi_r^* (1+g) + f(1-A_0)}{\cos\left[\bar{\theta}_{\max}^* / \bar{C} + 1\right]}$
Guo et al. (Guo et al., 2019)	$\tau = f(\sigma - \sigma_j) + \tau_j$
Note	where $\theta_{\max}^*$ is the greatest viewing dip angle. C represents a "coarseness" parameter. φ_r^* denotes the residual friction angle. σ_t denotes the compressive strength achieved from a standard uniaxial test. A_0 is the greatest virtual contact region. C denotes the coarseness parameter. B is a dimensionless fitting parameter. i_{ave} denotes the micro-average inclination angle calculated from the digitized data. $\overline{\theta_{3s}}$ is the effective three-dimensional mean slope angle. R_s denotes the coarseness coefficient. A_0 is the greatest contact region ratio. A_{jq} is the shear area of the fracture surface. A_{jj} represents the partial cementation surface area. R_{JRC} is the roughness coefficient. c_j and φ_j are shear strength parameters.

RMFJF experiments

Several scholars have conducted numerous experimental studies on the impacts of the filling degree and filling materials on the mechanical behaviors of RMFJFs. Guo et al. (2019) artificially created rough joints, filled the joints with sand particles of different sizes, and investigated the relationships between displacement, gap width, and flow. The stress-displacement curves of the unfilled joint fracture rock mass subjected to shear were divided into five stages: compression, elasticity, yielding, softening, and residual. However, the full curve of the RMFJF had only two stages, compression and hardening, which exhibited strain-reinforcement properties that resembled those of the curve of soft rock shear deformation (Liu et al., 2017).

Some scholars found that the shear strength decreased sharply when the filling degree was greater than 50%, and a model of the joint surface and intact rock sample damage was proposed. Moreover, the shear force was scarcely affected by the filling percentage when the external force increased to a certain value (Ladanyi, 2006). Pereira (1997) used sand grains 0.074-1.0 mm in size to fill granite joints and reported that when the filling percentage was greater than the sand grain size, the rolling friction controlled the mechanical behavior, leading to different degrees of decrease in the shear strength and friction coefficient. However, Guo et al. (2019) adopted four kinds of sand with different friction coefficients to fill joints and found that the peak shear stress in RMFJF was lower than that in unfilled RMFJF; this difference was considered to be caused by the shift of sand grains from rolling friction to sliding friction with increasing shear deflection. The peak shear intensity (Eq. (9)) of the unfilled jointed rock sample and the peak shear intensity (Eq. (10)) of the RMFJF expressed by the sand friction coefficient were obtained as follows:

$$\tau = \sigma \tan\left[\varphi_b + \frac{\arccos(1/R_s)}{(1+\sigma)^m}\right] \tag{9}$$

$$\begin{cases} \sigma_j = 523.53 e^{-6.45 f_s} \\ \tau_j = 125.24 e^{-4.93 f_s} \\ f = 7.12 f_s^2 - 8.55 f_s + 2.92 \\ \tau = f(\sigma - \sigma_j) + \tau_j \end{cases} \tag{10}$$

where R_s is the area ratio of the three-dimensional contour; φ_b denotes the friction angle of the joint surface; $\arccos(1/R_s)$ is the average climbing angle; $(1+\sigma)^m$ is the degree to which the normal stress decreases with respect to the climbing angle; f is the slope of the shear intensity line of the joint sample; f_s is the slope of the shear intensity line of sand; and σ_j and τ_j denote the horizontal and vertical coordinates of the intersection of the two shear intensity lines, respectively.

Using the volume averaging method, Minale (2014) deduced the momentum balance on a porous medium-solid skeleton. Moreover, there was no stress change when the stress was applied to the fluid or the rock skeleton. The total stress at the interface remained constant, and the stress at the interface was considered to be shared by

the rock and the fluid. The above studies showed that the mechanical behavior of RMFJFs was correlated with that of unfilled RMFJFs. The geological conditions under which RMFJFs develop are complex; the materials composing the RMFJF are diverse, and the material strength, thickness, and filling degree determine the mechanical behavior of the RMFJF.

Dynamic coupling relationship between filling body and surrounding rock

Closure effect of RMFJFs

If the rock matrix is regarded as isotropic, the RMFJF can exhibit anisotropy. During tectonic geostress, the RMFJF always experiences fissure generation, development, and closing. In this process, the mechanical characteristics, gap width, and porosity of the filling of the sample exerted important influences on the deformation and seepage properties of the rock mass. Therefore, it was important to study the constitutive relationship of the closure effect. Goodman conducted experiments on specimens with artificial fractures, and they found that the closure curve was nonlinear due to the tension at the interface. Some scholars conducted the coupled interaction of deflection and hydraulic conductivity of joint fractures, and they found that the closure curve was nonlinear within the elastic phase (Zhang et al., 2023). From the perspective of micromechanics, the fissure surface morphology of different parent rocks was mathematically described, as shown in Table 2, and most of the nonlinear deformation associated with joint fissure closure was reversible.

Relationship between RMFJF and surrounding rock

Several scholars have investigated the mechanical properties of preset strips and cylindrical RMFJFs. Li et al. reported that the lower the elastic modulus of the parent rock and filling material was, the less effect the filling material had on the pre-peak plasticity of the anchored rock sample. Therefore, considering the cooperation of the strength of the fillings and parent rock was important for determining the damage mode of the rock specimen (Zhang et al., 2012).

Tab. 2. Common empirical models for fracture closure.

Name	Model	Formula
Bandis (Bandis, 1980)	Hyperbolic model	$\delta = \frac{a\sigma}{b+\sigma}$
Malama and Kulatilake (Malama and Kulatilake, 2003)	Exponential model	$\delta = c\left(1-e^{-\sigma/d}\right)$
	Improved exponential model	$\delta = c_1\left[1-\exp\left(-\sigma^n/f\right)\right]$
Shehata et al. (Shehata et al., 2010)	Semilogarithmic model	$\delta = a_1 + b_1 \ln\sigma$
	Improved semilogarithmic model	$\delta = a_1 + b_1 \ln\left(\sigma + c_1\right)$
Sun and Xu (Sun and Xu, 1990)	Power model	$\delta = m\sigma^k$
Note	where δ is the closed deformation. σ represents the positive stress, and the remaining letters are empirical parameters.	

The RMFJF can be deemed a construction consisting of two parallel plates and fillings. Therefore, Ghazian and Ashjaee studied the flow characteristics of a fluid through partially filled channels. The free space size directly affects viscous dissipation. An increase in the Brinkman variable or a decrease in the Darcy variable will cause additional dissipation. Wang et al. (2023a) revealed that filling can improve the capacity of a sample to counteract cracking. The intensity of the samples in the curve decreased faster when the critical value of the friction angle was reached. The closer the strength of the filling was to that of the parent rock, the more obvious the reinforcement effect was. Moreover, the reinforcement effect was closely related to the rock bridge angle. When the rock bridge angle was 30°, the highest increase was 48.1%, as shown in Fig. 3.

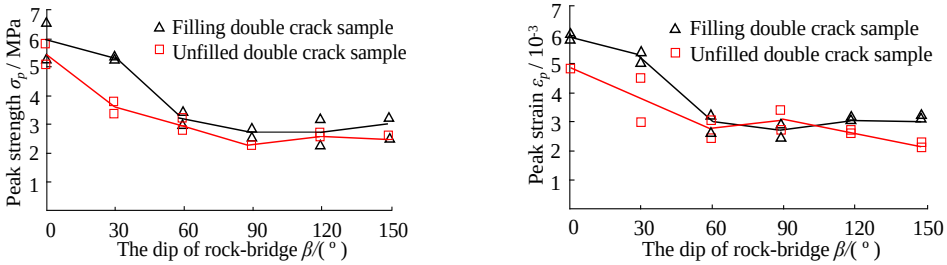

(a) Peak strength *(b) Peak strain*

Fig. 3. Effect of the rock bridge dip angle on the rock mass performance (Wang et al., 2023a).

Yan et al. (2023) reported that grouting increased the sample deformation resistance, shear strength, and residual strength, as shown in Fig. 4. The stress-displacement curve of the RMFJF could be divided into micro dislocation, explosive growth, weakening, and residual stages, as shown in Fig. 5. The filling cohesion can affect the damage mechanism of the rock sample (Zhang et al., 2012). Sample damage occurs mainly at the interface and within the grouting material and can form a cleavage plane penetrating the sample when the rock content is not too high. This difference might be caused by the lower strength of the filling compared with that of the parent rock.

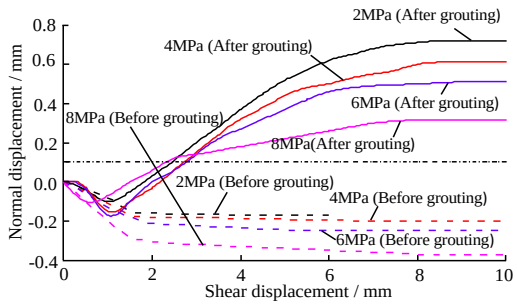

Fig. 4. Curves of shear-normal displacement (Yan et al., 2023).

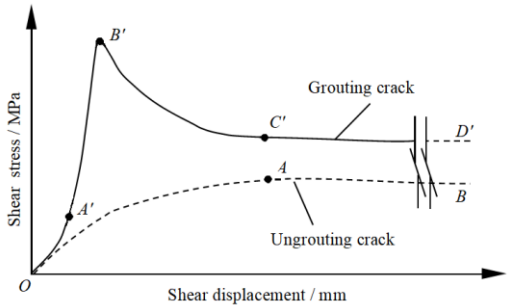

Fig. 5. Curvec of shear stress-shear displacement (Yan et al., 2023).

Considering the conservative effect of the JRC-JCS shear strength model. Zhang et al. (2012) made irregular jointed rock samples according to the Barton curve and reported that both the sample cohesion and friction angle were logarithmically related to the R_{JRC}, and the shear dilation phenomenon of the structural surface tended to increase with increasing specimen roughness. The presence of filling did not affect the location of fracture generation but could effectively inhibit the occurrence of stress convergence at the apex of fracture. Recently, through computed tomography (CT) scanning, Guo et al. (2017) reported that the slurry filling rate and solidification rate in fine fractures in rock samples after filling were greater than those in wide fractures, in which the fractal dimension of the joint surface decreased from 1.27 to 1.42 to 1.01 to 1.21, indicating that the filling effect was impressive and that the integrity of the rock mass improved.

In summary, the fractures that formed by Brazilian splitting were extremely close to natural fractures, but these fractures still cannot fully reflect the joint occurrence in in-situ engineering. Therefore, nondestructive in situ sampling and investigation of mechanical properties after filling could provide great guidance for in situ engineering. It was very difficult to study the microscopic phenomena of the test process and results previously. Fortunately, CT technology will improve this traditional drawback and open another window for in-depth study of the internal structure in geotechnical engineering.

Properties of RMFJF under cyclic shear load

At present, most studies on the RMFJF are based on static or quasistatic loading effects. The failure mode of RMFJF is a combination of filling and parent rock properties, and the contribution of each factor to failure should be considered comprehensively. Zhang et al. (2015) reported that the peak shear intensity of an RMFJF was impacted by the shear speed and filling. The shear strength changed more slowly than that of the unfilled rock sample. It decreases after each shear, and the fluctuation angle is proportional to the shear capacity. When the shear rate was below the critical value, its effect on the shear intensity of the sample was small, the critical value was determined by the parent rock properties, and the friction angle of the sample was smaller at higher shear rates. Tiwari et al. (2024) found that the parent rock strength and shear rate strongly impact the mechanical behavior of specimens, and others have reported that the peak shear strength occurs at a fluctuation angle of 30° and a shear speed of 1.01 mm/min. Considering the effect of fracture surface coarseness, the shear intensity of the specimens was negatively associated with the shear rate. He et al. (2023) obtained an equation for the shear strength of an

RMFJF under different shear rates. On the basis of the previous research of Ladanyi, Papaliangas et al. (1993) assumed that the peak decrease in shear intensity owing to circulative shear follows the hyperbolic model, and when the original positive stress was applied under CNS, the peak shear intensity formula of RMFJF after *N*-shaped circumferential shear can be expressed as:

$$\tau_p^{ci} = \sigma_{n0}\left(\frac{1.8}{1+k}\right)^{c_0}\left[\tan(i_0+\varphi_b)+(1-k)\alpha+\tan\varphi_{fill}^{\beta}\right]+c_{fill}-\sigma_{n0}\frac{N-1}{\alpha_N(N-1)+\beta_N} \tag{11}$$

In contrast to the model proposed by Indraratna, which can be represented by $\tau_p^{ci}=\tau_p^{mi}-\Delta\tau_i$, which was constructed based on regular jagged joints, the filling degree was not greater than the critical value; these models have deficiencies similar to those of the Ladanyi model; where τ_p^{ci} is the shear intensity peak value of the specimen after the *i*-th cyclic load; τ_p^{mi} represents the initial shear intensity peak of the specimens; $\Delta\tau_i$ is the peak value reduction in the shear strength after the *i*-th circular shear; N denotes the shear times; and α_N, β_N and c_0 are fitting constants and should be determined according to the cyclic shear test.

The shear rate could have an effect on the stability of RMFJF. Liu et al. obtained a stress-strain curve of rock specimens consistent with the shear failure mode, including three stages of elasticity, transition, and slip. The change trends of the shear strength and internal friction angle were positively related to the shear rate and inversely proportional to the filling degree (Liu et al., 2017). She and Sun (2018) derived the peak shear intensity of RMFJF with cement slurry under the three-dimensional morphological parameters shown in Eq. (12) from the peak shear intensity formula of two-dimensional regular dentate rock samples shown in Eq. (13). The error between the theoretical and experimental values approximately obeyed a Gaussian distribution.

$$\begin{cases}\tau_p=\sigma_n\tan(i+\phi_b)+\dfrac{cA_1}{A_0(\cos i-\sin i\tan\phi_b)}\\ i=\dfrac{1-4\alpha}{\sqrt{D_{SRA}-1}}e^{A_{SRA}}e^{\frac{\alpha D_{SRA}A_{SRA}}{1-\sigma_c'/\sigma_n}}\end{cases} \tag{12}$$

$$\tau_p=\sigma_n\tan(i+\varphi_b)+\frac{cl_1}{l_0(\cos i-\sin i\tan\varphi_b)} \tag{13}$$

where i denotes the dilatancy angle; σ_c' represents the compressive strength; and D_{SRA} is the fractal coarseness dimension.

When the filling percentage was lower than the threshold level, the peak shear intensity of hard rock diminished with the filling degree, while that of soft rock increased with the filling percentage. When the filling percentage was greater than the threshold level, the peak shear intensity of both the hard and soft rocks tended to stabilize (Fig. 6).

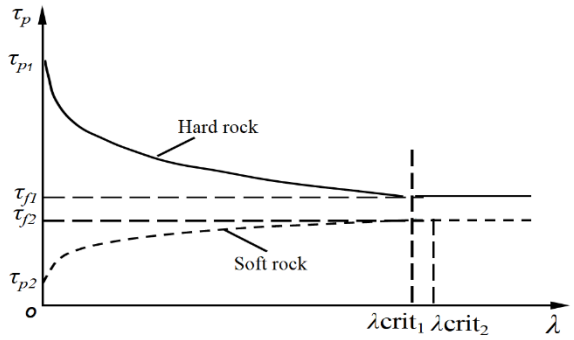

Fig. 6. Relationship between the shear strength and filling of the RMFJF (She and Sun, 2018).

Mechanical properties of RMFJF under impact loading

The impact load acting on the RMFJF consists mainly of rock bursts, earthquakes, and blasting, which are characterized by high energy and short durations. The filling enriches the composition of the rock mass, which causes the transmission path of a shock wave to be more complicated (Gong et al., 2022; Kang et al., 2023; Wang et al., 2023b).

Li et al. 2015 investigated the spreading law of shock waves in RMFJFs under dynamic loading in recent years. Liu et al. further investigated the spreading law of blasting stress waves via numerical simulation. Li et al. (2015) treated the RMFJF as thin layers and explored the propagation law of stress waves at one- and two-filling

fracture surfaces on the basis of the thin layer principle with an improved Hopkinson bar device. The filling degree has a great impact on stress wave propagation. The occurrence of fillings during geotechnical blasting can lead to the discharge of explosive energy, which makes it difficult to control the flatness and fragmentation of the contour surface after blasting and even produces flying stones. In contrast, the presence of fillings in demolition blasting can attenuate the effects of touchdown vibration on buildings, which has positive implications for safety protection.

A Hopkinson bar was used as the power source to investigate the effect of filling thickness on the stress wave spreading law. Li et al. (2018) reported that an increase in the filling degree causes a decrease in the sample's initial stiffness and shockwave transmittance, and an increase in the stress amplitude causes nonlinearity in the mechanical behavior and an increase in the stiffness of the filling medium. Yang et al. (2016b) found that the samples were mainly subjected to tensile damage. The dynamic elastic modulus was positively related to the shock wave speed. The filling had a significant barrier influence on the spreading law of the stress wave, and the energy dissipation ratio was determined by the mechanical properties of the fillings. Along with the decrease in filling strength, the attenuation of the stress wave becomes more obvious, and the change laws of the reflection power and transmission power show opposite trends.

Through the dynamic characteristics of parallel unequally spaced RMFJFs, it was found that the greater the filling degree of samples under low-velocity impact loading was, the stronger the reflection ability was, and the greater the attenuation degree of the shock wave was. Simultaneously, the reflection energy ratio and the dissipation energy ratio increase. Through the test of rock samples with different concave and convex numbers and contact areas, it was found that the loading frequency had an effect on the closure deformation. The connection between the sample parameters and load frequency was also obtained. Moreover, the constitutive model of the RMFJF under different loading frequencies was modified (Liu et al., 2014). The RMFJF under impact loading mainly focuses on the propagation behavior of impact waves. However, the structural response of the surrounding RMFJF after a rock burst is worthy of attention.

Numerical simulation of properties of RMFJF

Parameter selection is crucial to the numerical study of RMFJF because it is the key to characterizing the actual features of the sample. Finite element software can be used for numerical simulation after macroscopic parameters are obtained, while the mesoscopic parameters of the particles need to be provided via PFC or other discrete element software. At present, there is no clear conversion law between macroscopic and mesoscopic parameters, and trial and error testing is still used to change mesoscopic parameters until the requirements are repeatedly met (Li et al., 2015). With the help of PFC2D, the sample shear strength was negatively correlated with the size of the filling particle, and the friction angle decreased with increasing contact rigidity ratio, decreased and then increased with increasing parallel bond rigidity ratio. In addition, the contact between the particles was found to have little effect on the sample cohesion. Tian and Yang (2017) found that the peak shear intensity and elastic modulus of RMFJF were lower than those of the intact sample. The peak strength reached the maximum and minimum values at ligament angles of 120° and 60°, respectively, as shown in Fig. 7.

The fish were embedded in PFC2D software. Li et al. (2015) reported that the Patton strength model was suitable for describing wear damage, whereas the Ladanyi model was suitable for describing shear damage (Fig. 8). Rock fissure propagation was closely related to the stress state. Normal cracks played a dominant role in the elastic range. After the stress reaches the peak value, the tangential crack develops rapidly, and the P and R cracks ultimately connect with each other in the later stage until the rock mass is destroyed and becomes unstable. Zhang et al. (2023) discovered that the filling degree had less effect on the damage mode of samples with the same roughness. When the roughness was between 6 and 8 and the filling thickness was greater than the undulation angle, the filling thickness was negatively correlated with the peak shear intensity and remanent intensity of the sample. However, when the filling thickness was less than the undulation angle, the specimen could produce new fissures at larger undulation angles that gradually penetrated to the bottom. As the filling thickness increases, fissures are still produced but do not penetrate (Figs. 9 and 10).

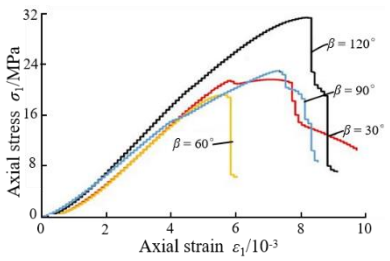

Fig. 7. Axial stress-strain curve of RMFJF (Tian and Yang, 2017).

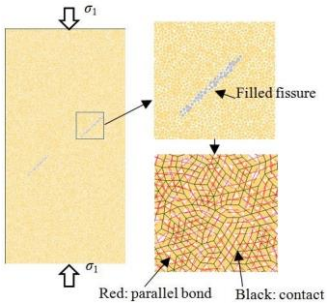

Fig. 8. Numerical modeling of RMFJF (Li et al., 2015).

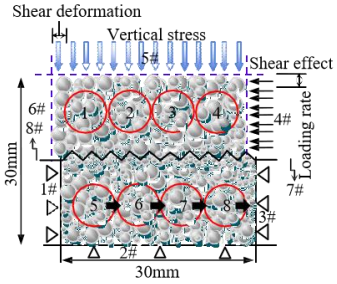

Fig. 9. Shear test simulation model with PFC (Zhang et al., 2023).

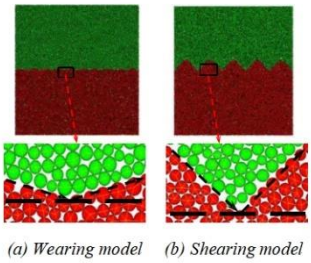

Fig. 10. Joint settings for different test models (Zhang et al., 2023).

Xu et al. (2018) combined PFC2D and a fish program to prove the reliability of the calculation results, as shown in Figs. 11 and 12. They found that the JRC had an unusual effect on the peak shear intensity of a rock mass. The peak shear strength was proportional to the filling strength, the cohesion was proportional to the contact surface bond strength, and the friction angle was inversely proportional to the contact surface bond strength. The shear strength and other mechanical parameters of the samples significantly improved after the joint fissures were filled with cement slurry (She et al., 2018). When the filling percentage was higher than 100%, the variation in the mechanical parameters could be ignored, indicating that the natural fractures had propagated at this time.

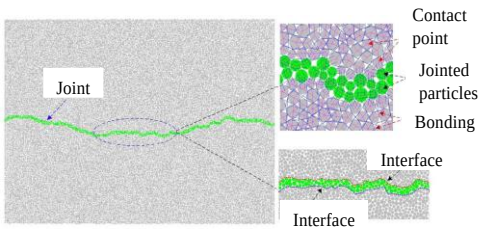

Fig. 11. RMFJF model with JRC from 14 to 16 (Xu et al., 2018).

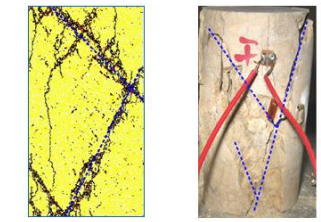

Fig. 12. Damage patterns of specimens (Xu et al., 2018).

The commonly used methods for generating random fractal curves include the Brownian motion method, Weierstrass function method, and Hurst exponent method. Several studies have applied the Weierstrass function method to form curves with varied fractal parameters and carried out numerical studies with a fractal dimension D=1.1 to obtain empirical formulas for the friction coefficient, cohesion, and filling degree. A combination of experiments and COMSOL Multiphysics numerical analysis was used to visualize the permeability coefficients and flow paths in the contact area of rock samples subjected to shear beneath the CNL and CNS boundary constraints. It was established that sample coarseness had an important effect on the shear expansion and the flow paths. Several scholars have used ABAQUS to construct rock samples containing both anchored and filled specimens and found that the simulation results were consistent with the physical experiments (Guo et al., 2019). The Bandis formula is commonly used in engineering to study the shear strength of rock masses, while in numerical simulations, the stiffness parameters are always simplified as constants, reducing the results' reliability. Qi used 3DEC and the built-in fish program to customize the constitutive model of the joint surface, modified the stiffness parameters, and finally obtained the modified Bandis empirical formula, which describes the dynamic variation in shear stiffness with normal stress (Qi et al., 2014).

The shear intensity of the RMFJF was affected by the fracture surface profile, fillings, and mechanical behaviors of the parent rock. Laboratory experiments are a common means of investigating the mechanical behaviors of RMFJFs, through which intuitive and accurate results can be obtained. However, related research from a mesoscopic point of view is greatly limited. Fortunately, numerical simulations have enriched this research; however, how the results can truly reflect the rock mass characteristics in practical engineering is intimately associated with establishing random fissure networks and calibrating rock mechanical parameters. Moreover, since each joint surface is unique, the reliability of the shear seepage properties of large-scale fractured rock masses determined by using fractal topology to calibrate parameters requires further investigation.

Seepage characteristics of RMFJF

Seepage characteristics of RMFJF

The permeability coefficient can reflect the groutability of a rock mass. Jones et al. considered the association between effective stress and the permeability coefficient as a negative power exponent, while their relationship in the Louis formula was described by a negative exponential function. At present, the change in the permeability

coefficient is mainly described by the strain. In addition, several scholars have proposed the evolution pattern of the permeability tensor in the EDZ region. However, a few academics have used stress to describe the evolution equation of the permeability coefficient (Ma, 2015). Whether the above results can be directly applied to analyze the permeability evolution of RMFJFs needs further verification.

Studying the nonlinear behavior of fluid in fracture space by simplifying the Navier–Stokes equation and cubic law is a good approach. Chen and Zhang found that the tension and shear effects generated by expansive fillings caused a marked increase in the permeability of the sample. Moreover, the plasticizing and liquefying effects of the fillings have a positive influence on increasing the permeability of the sample, and the expression can be described as follows (Chen et al., 2016):

$$\Delta K_J = \frac{n\beta w^3}{L-\Delta L} - \frac{n\beta w^3}{L} \tag{14}$$

where w is the initial width of the fissure and n denotes the porosity of the filling; β is the correlation coefficient; L represents the fissure length; ΔL is the variation in fracture length.

As shown in Eq. (14), the permeability coefficient increases by 8 times when the fissure width doubles. Therefore, it is crucial to consider fluid-structure interactions when studying RMFJF groutability because a small change in fissure width significantly affects the permeability of a rock mass.

Based on the continuity equation, Navier-Stokes equation, and generalized Brinkman equation, Shu et al. reported that the discrepancies between the theoretical values and experimental results of equivalent permeability were very small, within an order of magnitude (Shu et al., 2018). This research assumed that the joints extended infinitely along the X-direction, the flow velocity at the intersection was equal, and the shear stress was continuous.

The effective permeability K_x of the partial RMFJF may be expressed as follows:

$$K_x = \frac{1}{H}\left[\frac{(1-\xi)^3 b^3}{12} + \xi b K_1 + (H-b)K + \frac{(1-\xi)b}{2}(K_1+K_2) - \frac{2(K_1-K_2)^2}{\sqrt{n_1 K_1}+\sqrt{n_2 K_2}}\right] \tag{15}$$

When ξ=0, the joint fissure was not filled. Then, K_x may be simplified as follows:

$$K_x = \frac{1}{H}\left[\frac{b^3}{12} + \left(H-\frac{b}{2}\right)K_2 - 2\sqrt{\frac{K_2^3}{n_2}}\right] \tag{16}$$

When ξ=1, the joint fissure was completely filled. Then, K_x can be simplified as follows:

$$K_x = \frac{1}{H}\left[bK_1 + (H-b)K_2 - \frac{2(K_1-K_2)^2}{\sqrt{n_1 K_1}+\sqrt{n_2 K_2}}\right] \tag{17}$$

where b is the fissure aperture; H denotes the sample thickness; n_1 is the porosity of the filling; K_1 denotes the permeability of the filling; n_2 is the porosity of the bedrock; K_2 represents the permeability of the bedrock; and ξ is the filling degree.

Ye et al. (2019) considered a rock mass to be composed of three parts: parent rock, fillings, and free space. The fluid flow was assumed to be infinite along the X-direction, and the joints were expanded infinitely. The fluid was considered an incompressible Newtonian fluid and satisfied the continuity equation. The fluid velocity and shear stress at the interfaces remained continuous. The fluid velocity expression in the corresponding space was obtained as follows:

$$\begin{cases} v_x = -\dfrac{\Delta p}{2L\eta}y^2 + A_1 y + A_2 & \text{(Free fracture flow)} \\ \mathrm{u}_x = B_1 \mathrm{e}^{\sqrt{n_1/K_1}y} + B_2 \mathrm{e}^{-\sqrt{n_1/K_1}y} + \dfrac{\Delta p K_1}{L\eta} & \text{(Flow in the filling)} \\ w_x = C_1 \mathrm{e}^{\sqrt{n_2/K_2}y} + C_2 \mathrm{e}^{-\sqrt{n_2/K_2}y} + \dfrac{\Delta p K_2}{L\eta} & \text{(Flow in the parent rock)} \end{cases} \tag{18}$$

By integral treatment of the flow velocity v_x in Eq. (18) and parameter equivalent replacement, the permeability coefficient expressions in the x and y directions were obtained together as follows:

$$\begin{cases} K_x^* = \dfrac{L\eta}{\Delta p}\bar{V}_x = \dfrac{1}{H}[\dfrac{K_1^2 - K_2^2}{\sqrt{n_1 K_1} + \sqrt{n_2 K_2}} + K_1 \xi b + \\ K_2(H-b) + \dfrac{b(1-\xi)}{2}(K_1 + K_2) + \dfrac{b^3(1-\xi)^3}{12}] \\ K_y^* = k_y \dfrac{\eta}{\gamma_w} = \dfrac{H}{\xi b / K_2 + (H-b)/K_1} \end{cases} \tag{19}$$

where Δp is the pressure gradient, and L denotes the seepage range; A_1, A_2, B_1, B_2, C_1 and C_2 are test coefficients; η is the dynamic viscosity; n_1 and n_2 represent the porosities of the bedrock and filling material, respectively; and K_1 and K_2 represent the permeabilities of the filling and bedrock, respectively.

Based on Eq. (19), after collecting the seepage volume at multiple time points, it was found that although the experimental value was slightly larger than the calculated value by equivalent conversion, which gradually increased with time and became more obvious at 1800 s and reached the greatest value at 3000 s, as shown in Fig. 13 (Ye et al., 2019), it was evident that the theoretical solution of the effective permeability factor was reasonable. Takemura et al. (2010) obtained semiempirical permeability formulas for rock samples considering the filling particle size and porosity. Adopting Darcy's law to characterize the flow property when the liquid moved in a high-porosity medium was unsuitable. The first-order Darcy equation has difficulty describing the higher-order nature of fluid motion, which can lead to the contact surface stress discontinuity. Brinkman modified Darcy's law with a factor containing a second-order viscous term. The fluid motion in the unfilled part of a rock mass can be characterized by the Navier-Stokes formula. Due to the difficulty of dealing with contact conditions, an empirical constant was introduced in the solution to study the velocity distribution of the fluid on the contact surface by using the stress jump boundary.

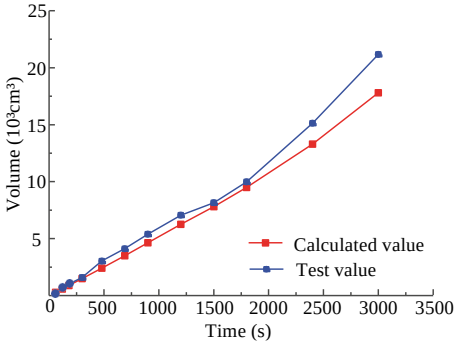

Fig. 13. Comparison of calculation and test results (Ye et al., 2019).

Moreover, double-domain and single-domain methods were used to analyze viscous fluid motion. To analyze the temporal stability of the similarity solution of incompressible fluid flow in an RMFJF, a similarity transformation that fulfills both the Navier–Stokes equation of fluid flow in free space and the extended Darcy's law of Brinkman in dense parent rock was proposed. Guo et al. (2019) reported that the exponential order between the unit head flow rate of random fracture and the mechanical gap width was 3.01, which approximately satisfied the cubic relationship. The equivalent permeability expression for the RMFJF can be derived based on the tensor and generalized cubic law. Mamot et al. (2018) reported that when ice was used as a filling material, its initial damage had a greater effect on the integrity and stability of RMFJF. An improved Mohr-Coulomb damage criterion was then established by considering the effects of temperature and stress.

Laboratory test on seepage characteristics of RMFJF

Although 3D-printed specimens have defects such as low strength and ductility, the generation and development path of simulated joints in dynamic tests in SHPB matches well with the rock samples taken in the field. Based on the conventional modeling method and sophisticated printing technology, the internal structure of the RMFJF can be reconstructed so that the development of the interior fissure network of the rock mass can be intuitively observed. Many scholars have used 3D printing to produce inserts to characterize high-precision joint fracture surfaces and then cast the parent rock with rock-like material and the space occupied by the insert with another material. The internal fracture structure of visual coal rock samples can be obtained by printing different

materials (Kim et al., 2016). Head and Vanorio (2016) tested the porosity, pore structure, and permeability of 3D-printed specimens and investigated the fracture deformation and fluid flow properties of rock samples.

With the help of 3D-printing technology, Wang et al. (2022) constructed rock samples with different penetration rates and fillings of unequal width; it was found in the following experiment that the sample permeability increased exponentially with increasing penetration rate. The permeability coefficients of rock samples containing unequal width fillings showed a quadratic relationship with the unequal width ratio. Liu et al. (2014) reported that joint occurrence affects the permeability of samples, and the effect order from the largest to smallest can be ranked as follows: double-wide joint fissure, single-wide joint fissure, and cross-joint fissure. The permeability variations were on the same order of magnitude. Moreover, high seepage occurred in a short time in rock masses containing elastic-plastic filling, while it lasted for a long time in those containing brittle filling. The fractures gently closed with the increase in surrounding stress, and the influence of gap width and roughness on permeability was greatly weakened. During the unloading period of surrounding stress, permeability differences exist among the different samples in view of the change in the surrounding stress.

The seepage flow was related to the axial pressure and fracture depth, and the surrounding stress also had a meaningful influence on the seepage flow of the samples (Head and Vanorio, 2016). By calculating the morphological value of the irregular fracture surface, it was found that an exponential function and a power function can describe the interrelation between the seepage quantity and permeability force when the confining pressure and permeability pressure are constant. The concept of an effective critical point for seepage control was then proposed, and the relationship between the seepage parameters of the RMFJF and porous media was derived. The above results indicate the importance of 3D-printing technology in practical projects and increase scholarly confidence in further studies of deep geotechnical engineering.

Problems and development trends of RMFJF

At present, clay is mostly used as a filling material for researching the mechanical behavior of RMFJF, which has a meaningful effect on the reliability of rock masses due to its poor permeability, decreased strength in water, and tendency to cause high superpose water pressure. When a hard material is used to fill a joint, the filling composition, fracture roughness, and the interaction between the parent rock also have meaningful effects on the mechanical behaviors of the specimens. For the specimens containing hard fillings, the coarseness of the fracture surface hinders the migration of the filling particles, and the fewer the coarseness is, the lesser the constraint on the filling particles. However, investigations on the mechanical behaviors of RMFJFs below the coupling induction of fillings and parent rock have been insufficient. First, efforts should be made to clarify the strength grade of the parent rock, and then a series of filling tests can be performed to study the mechanical behaviors in detail (Li et al., 2022; Gong et al., 2023).

It is generally believed that the closure of the RMFJF is stronger than that of unfilled rock samples. For the latter, some scholars often use strain to describe the evolution of the permeability parameter. To date, there has been insufficient research on the self-closing behavior of RMFJF, whether through theoretical analysis, experimental investigation, or numerical studies. The geostress applied by an RMFJF can be divided into static and dynamic states, but research on the mechanical properties of an RMFJF under cyclic loading and impact loading is insufficient. Although impact loads cannot act on an RMFJF too much, special attention should still be given to this phenomenon in future research because impact loads considerably affect the stability of a rock mass and can cause catastrophic consequences once they occur. Several scholars use regular serrated triangular shapes to characterize joints to ensure the accuracy of the filling degree and the stability of the undulating angle. However, natural joints are characterized by both an undulation degree and roughness. Although the ISRM has affirmed the quantitative characterization of joint roughness by JRC, numerous difficulties still exist in modeling three-dimensional rock samples. Therefore, accurately controlling the filling degree of the RMFJF and characterizing the joint randomness are important issues for future research.

3D-printing technology violates the traditional methods for sample fabrication. Although there was a disparity between the sample and the practical rock in terms of rock brittleness (Amin et al. 2024), the former performed well in refining joint production and development, making the volatility and coarseness of the lower strength of the sandstone sample infinitely approach those of practical joints. In traditional research, endless limitations, such as time consumption, model replication difficulty, or easy destruction of the joint surface, always exist in the process of field testing, in situ sampling, and sample fabrication and can result in large errors in the results. The defects of 3D-printed specimens are related to the printing resolution and material properties. The printing resolution impacts the accuracy of the specimen size, and the material properties determine the properties of rock samples. Therefore, these defects will be gradually solved with technological development. 3D printing can help scholars break the black box of geotechnical engineering research and become a powerful tool for in-depth study of geotechnical engineering.

Conclusions

This study summarizes the status of research on the shear seepage characteristics of RMFJF through experimental studies, numerical studies, theoretical model studies, and the dynamic coupling relationship between fillings and surrounding rock loads. The main conclusions are as follows:

(1) The filling mechanical properties directly affect the permeability and groutability of specimens. It is crucial to select appropriate materials as fillings and then investigate their mechanical properties and coordinated deformation with bedrock.

(2) The occurrence relationship between joints and bedrock has a meaningful effect on the mechanical behaviors of specimens. It is indispensable to research further the impact of diverse roughnesses and their occurrence on the shear seepage characteristics of RMFJFs with the help of advanced technology.

(3) The seepage properties of specimens under cyclic and impact loading require detailed study. The detailed impact of temperature on the permeability characteristics of the RMFJF needs to be further studied.

Advanced science and technology, for instance, CT and 3D-printing technology, have been used to investigate the shear seepage behaviours of RMFJFs. They can partly visualize or dynamically present the specimens to the operators, which might help solve future challenges and become a potential method for further studies.

Reference

Amin, S. M., Desai, C. S., Zhang, L. Y., Hosseinali, M., Toufigh, V., Ghaemian, M. (2024). Experimental investigation and constitutive modeling of rock-like specimens interface with the effect of roughness based on 3d printing. International Journal of Geomechanics, 24(2), pp. 04023283. DOI: 10.1061/IJGNAI.GMENG-8823

Bandis, S. (1980). Experimental studies on shear strength-size relationships, and deformation characteristics of rock discontinuities. University of Leeds (United Kingdom), pp. 50-70.

Barton, N. (1973). Review of a new shear-strength criterion for rock joints. Engineering geology, 7(4). pp. 287-332. DOI: 10.1016/0013-7952(73)90013-6

Chen, J. G., Zhang, L., Fan, J. W. (2016). Seepage-stress characteristics of brittle-plastic filled fracture. Journal of Mining and Safety Engineering, 33(6). pp. 1103-1109. DOI: 10.13545/j.cnki.jmse.2016.06.021

Gong, J., Fang, D. L., Liang, W. M., Wang, S. R. (2022). Influence factors analysis of projectile kinetic energy at muzzle of magnetoresistive coil gun. Journal of Engineering Science and Technology Review, 15(6). pp. 170-177. DOI: 10.25103/jestr.156.21

Gong, J., Liu, Q. Q., Wang, S. R., Wang, Z. X., Li, C. L. (2023). Mechanical properties and microscopic mechanism of paper mill sludge-magnesium oxychloride cement composites. DYNA, 98(1). pp. 57-63. DOI: 10.6036/10714

Grasselli, G., Egger, P. (2003). Constitutive law for the shear strength of rock joints based on three-dimensional surface parameters. International Journal of Rock Mechanics and Mining Sciences, 40(1). pp. 25-40. DOI: 10.1016/S1365-1609(02)00101-6

Guo, B. H., Cheng, T., Chen, Y., Jiao, F. (2019). The seepage characteristics of marble fracture and the influence of filling sand soil. Shuili Xuebao, 50(4). pp. 463-474. DOI: CNKI:SUN:SLXB.0.2019-04-006

Guo, D. M., He, T. Y., Yang， R. S., Ye, S. D., Zhang, Y. Q., Li, X. P. (2017). CT analysis on micro-cement grouting effect for fractured rock sample. Journal of Mining and Safety Engineering, 34(5). pp. 987-992. DOI: 10.13545/j.cnki.jmse.2017.05.024

He, L., Lu, X., Copeland, T., Chen, J., Yan, J., Zhao, W. (2023). The impact of shear rate on the mechanical behavior of rock joints under multiple-influencing factors. Rock Mechanics and Rock Engineering, 56(10). pp. 7397-7414. DOI: 10.1007/s00603-023-03432-x

Head, D., Vanorio, T. (2016). Effects of changes in rock microstructures on permeability: 3-D printing investigation. Geophysical Research Letters, 43(14). pp. 7494-7502. DOI: 10.1002/2016GL069334

Kang, Y., Hou, C., Liu, B., Bai, W. (2023). Influence of water content on the shear strength of rock joints with clay-rich fillings. Rock Mechanics and Rock Engineering, 56(2). pp. 1437-1449. DOI: 10.1007/s00603-022-03158-2

Kim, D. H., Gratchev, I., Hein, M., Balasubramaniam, A. (2016). The application of normal stress reduction function in tilt tests for different block shapes. Rock Mechanics and Rock Engineering, 49(8). pp. 3041-3054. DOI: 10.1007/s00603-016-0989-x

Kyaw, P. P. S. S., Uchida T. (2023). Assessment of the breaching event, breach parameters and failure mechanisms of the spillway collapse in the Swa dam, Myanmar. Water, 2023, 15(8). pp. 1513. DOI: 10.3390/w15081513

Ladanyi, B. (2006). Creep of frozen slopes and ice-filled rock joints under temperature variation. Canadian Journal of Civil Engineering, 33(6). pp. 719-725. DOI: 10.1139/l05-112

Li, J. C., Liu, T. T., Li, H. B., Liu, Y. Q., Liu, B., Xia, X. (2015). Shear wave propagation across filled joints with the effect of interfacial shear strength. Rock Mechanics and Rock Engineering, 48(4). pp. 1547-1557. DOI: 10.1007/s00603-014-0662-1

Li, J. T., Li, D. Q., Wang, S. R., Chen, Y. B. (2022). Analysis of collapse mechanism and anti-collapse support of borehole in deep tectonic coal. Journal of Engineering Science and Technology Review, 15(6). pp. 125-131. DOI: 10.25103/jestr.156.15

Li, X. F., Li, H. B., Li, J. C., Zhao, J. (2018). Effect of joint thickness on seismic response across a filled rock fracture. Géotechnique Letters, 8(3), 190-194. DOI: 10.1680/jgele.18.00042

Liu, T.T., Li, J. C., Li, H. B., Li, X. P., Li, N. N. (2017). Influence of shearing velocity on shear mechanical properties of planar filled joints. Rock and Soil Mechanics, 38(7). pp. 1967-1973. DOI: 10.16285/j.rsm.2017.07.016

Liu, X. Y., Liu, A. H., Li, X. B. (2014). Experimental study of columnar jointed sand-stont-like material with preset filling. Chinese Journal of Rock Mechanics and Engineering, 33(4). pp. 772-777. DOI: 10.13722/j.cnki.jrme.2014.04.011

Lu, Y., Wang, L., Li, Z., Sun, H. (2017). Experimental study on the shear behavior of regular sandstone joints filled with cement grout. Rock Mechanics and Rock Engineering, 50(5). pp. 1321-1336. DOI: 10.1007/s00603-016-1154-2

Ma, J. (2015). Review of permeability evolution model for fractured porous media. Journal of Rock Mechanics and Geotechnical Engineering, 7(3). pp. 351-357.DOI: 10.1016/j.jrmge.2014.12.003

Malama, B., Kulatilake, P. H. S. W. (2003). Models for normal fracture deformation under compressive loading. International Journal of Rock Mechanics and Mining Sciences, 40(6). pp. 893-901. DOI: 10.1016/S1365-1609(03)00071-6

Mamot, P., Weber, S., Schröder, T., Krautblatter, M. (2018). A temperature-and stress-controlled failure criterion for ice-filled permafrost rock joints. The Cryosphere, 12(10). pp. 3333-3353. DOI: 10.5194/tc-12-3333-2018

Min, K. B., Jing, L. (2003). Numerical determination of the equivalent elastic compliance tensor for fractured rock masses using the distinct element method. International Journal of Rock Mechanics and Mining Sciences, 40(6). pp. 795-816. DOI: 10.1016/S1365-1609(03)00038-8

Minale, M. (2014). Momentum transfer within a porous medium I. Theoretical derivation of the momentum balance on the solid skeleton. Physics of Fluids, 26(12). pp. 57-74. DOI: 10.1063/1.4902955

Papaliangas, T., Hencher, S. R., Lumsden, A. C., Manolopoulou, S. (1993). The effect of frictional fill thickness on the shear strength of rock discontinuities. In International Journal of Rock Mechanics and Mining Sciences and Geomechanics Abstracts, 30(2). pp. 81-91. DOI: 10.1016/0148-9062(93)90702-F

Patton, F. D. (1996). Multiple modes of shear failure in rock. Proceedings of the First Congress of International Society of Rock Mechanics, Lisbon, pp. 509-513.

Pereira, J. P. (1997). Rolling friction and shear behaviour of rock discontinuities filled with sand. International Journal of Rock Mechanics and Mining Sciences, 34(3-4). pp. 244-e1. DOI: 10.1016/S1365-1609(97)00037-3

Premadasa, W., Indraratna, B. (2020). Discussion of numerical simulation of the shear behavior of rock joints filled with unsaturated soil by Libin Gong, Jan Nemcik, and Ting Ren. International Journal of Geomechanics, 20(4). pp. 07020002. DOI: 10.1061/(ASCE)GM.1943-5622.0001604

Qi, J. D., Jin, A. B., Wang, H., Gao, Y. H., Yu, Y. Y. (2014). Correction and application of the Bandis empirical formula. Journal of University of Science and Technology Beijing, 36(12). pp. 1575-1582. DOI: 10.13374/j.issn1001-053x.2014.12.002

She, C. X., Sun, F. T. (2018). Study of the peak shear strength of a cement-filled hard rock joint. Rock Mechanics and Rock Engineering, 51(3). pp. 713-728. DOI: 10.1007/s00603-017-1358-0

Shehata, I. A., Shehata, L. D. D., de Mendonça, E. C. G. (2010). Strength of shear keys used in pre-cast prestressed composite beams. Materials and Structures, 43(5). pp. 675-685. DOI: 10.1617/s11527-009-9520-0

Shu, F. J., Fu, W. X., Wei, Y. F., Xia, W. (2018). Theoretical analysis and experiment on seepage of rock mass containing periodic fractures with partial filling. Journal of Hunan University(Natural Sciences), 45(2). pp. 114-120. DOI: 10.16339/j.cnki.hdxbzkb.2018.01.015

Son, B. K., Lee, Y. K., Lee, C. I. (2004). Elasto-plastic simulation of a direct shear test on rough rock joints. International Journal of Rock Mechanics and Mining Sciences, 41. pp. 354-359. DOI: 10.1016/j.ijrmms.2004.03.066

Sun, Z. Q., Xu, F. M. (1990). Study of rock joint surface feature and it's classification. Study of rock joint surface feature and its classification. International Journal of Rock Mechanics and Mining Sciences and Geomechanics Abstracts, 27(6). pp. 101-107. DOI:10.1016/0148-9062(90)91126-R

Takemura, T., Osada, M., Fujii, Y., Kanamaru, T., Takahashi, M. (2010). Hydraulic properties of a single rock fracture filled by calcite. Journal of the Japan Society of Engineering Geology, 51(2). pp. 92-96. DOI: 10.1016/j.ijrmms.2006.11.001

Tian, W. L., Yang, S. Q. (2017). Experimental and numerical study on the fracture coalescence behavior of rock-like materials containing two non-coplanar filled fissures under uniaxial compression. Geomechanics and Engineering, 12(3). pp. 541-560. DOI: 10.12989/gae.2017.12.3.541

Tian, Y., Liu, Q., Ma, H., Liu, Q., Deng, P. (2018). New peak shear strength model for cement filled rock joints. Engineering Geology, 233. pp. 269-280. DOI: 10.1016/j.enggeo.2017.12.021

Tiwari, G., Kumar, A., Gali, M. L. (2024). Velocity-weakening tendency in rate-dependent strength behavior of soft rock-like joints. International Journal of Geomechanics, 24(1). pp. 06023025. DOI: 10.1061/IJGNAI.GMENG-883

Wang, K., Zhang, C., Gao, Y., Chen, H., Xie, T. (2023a). Influence of prefabricated fissure combinations on strength and failure characteristics of rock-like specimens under uniaxial compression. International Journal of Geomechanics, 23(2). pp. 04022279. DOI: 10.1061/(ASCE)GM.1943-5622.0002637

Wang, S., Zhang, J., Li, C., Li, Z., Yu, Y. (2022). Seepage characteristics of fractured rock mass with non-equal width filling under cyclic loading. Ain Shams Engineering Journal, 13(6). pp. 101794. DOI: 10.1016/j.asej.2022.101794

Wang, S. R., Zhao, J. Q., Gong, J., Xu, J. M., Li, C. L. (2023b). Analysis on energy absorption capacity of MLWC under electromagnetic driving SHPB condition. DYNA, 98(3). pp. 256-264. DOI: 10.6036/10824

Xia, C. C., Yue, Z. Q., Tham, L. G., Lee, C. F., & Sun, Z. Q. (2003). Quantifying topography and closure deformation of rock joints. International Journal of Rock Mechanics and Mining Sciences, 40(2). pp. 197-220. DOI: 10.1016/S1365-1609(02)00134-X

Xu, W. Z., Lin, H., Cao, R. H. (2018). Simulation and macro-mesoscopic parameter analysis for direct shear of filled rough joints. Journal of Southwest Jiaotong University, 53(3). pp. 548-557. DOI: 10.3969/j.issn.0258-2724.2018.03.016

Yan, L., Chang, J., Qiao, L., Shi, W., Wang, T., Pang, D., Li, Y., Guo, Y. (2023). Similar ratio experiment and characteristic analysis of quasi-sandstone. Frontiers in Earth Science, 10. pp. 1108582. DOI: 10.3389/feart.2022.1108582

Yang, J., Rong, G., Hou, D., Peng, J., Zhou, C. (2016a). Experimental study on peak shear strength criterion for rock joints. Rock Mechanics and Rock Engineering, 49(3). pp. 821-835. DOI: 10.1007/s00603-015-0791-1

Yang, R. S., Wang, M. Y., Yang, Y., Wang, J. G. (2016b). Simulation material experiment on the dynamic mechanical properties of jointed rock affected by joint-filling material. Journal of Vibration and Shock, 35(12). pp. 125-131. DOI: 10.13465/j.cnki.jvs.2016.12.019

Ye, F., Duan, J. C., Fu, W. X., Yuan, X. Y. (2019). Permeability properties of jointed rock with periodic partially filled fractures. Geofluids, 2019. pp. 4039024. DOI: 10.1155/2019/4039024

Zhang, B., Li, S. C., Yang, X. Y., Wang, B., Li, M. T. (2012). Influence of crack fillings to rock uniaxial compression mechanical property and anchoring effect. Journal of China Coal Society, 37(10). pp. 1671-1676. DOI: 10.13225/j.cnki.jccs.2012.10.009

Zhang, J. L., Shen, M. R., Liang, Z. R. (2015). Experimental study on shear strength characteristics of irregular rock mass discontinuities, Journal of Southwest Jiaotong University. 50(6). pp. 993-1000. DOI: 10.3969/j.issn.0258-2724.2015.06.004

Zhang, Y., Zhang, W., Wang, L., Xiao, T., Meng, X., Zhang, Z. (2023). Mechanism of the high-speed and long-run-out landslide considering the evolution of the frictional heat in the sliding zone. Natural Hazards, 2. pp. 1-19. DOI: 10.1007/s11069-023-06334-x